CMS Physics Analysis Summary

Contact: cms-pog-conveners-lum@cern.ch 2018/06/06

CMS luminosity measurement for the 2017 data-taking period at $\sqrt{s} = 13$ TeV

The CMS Collaboration

Abstract

The calibration for the luminosity measurement by the CMS experiment for the 2017 proton-proton LHC run at $\sqrt{s} = 13$ TeV is described. The principal calibration is derived from the analysis of the van der Meer scan program in CMS taken during LHC fill 6016. In addition, the performance and stability of the CMS luminometers are also evaluated using emittance scans taken throughout the course of the year. The systematic uncertainty in the absolute calibration from the van der Meer scan is derived with a precision of 1.5%, with the dominant contributions arising from the x-y correlations of the beam shape and the scan to scan variation. The total systematic uncertainty, including terms from stability and linearity effects, is 2.3%. The uncertainty for the special low-pileup run at the end of 2017 is also evaluated and found to be 1.7%.

1 Introduction

Precision measurement of the luminosity delivered to the CMS experiment [1] by the LHC is important for a variety of reasons. Online, the luminosity measurement provides realtime feedback on the LHC performance and operation, as well as to CMS operations for tasks such as measurements of trigger rates. Offline, the luminosity measurement is a crucial component of nearly every physics analysis, either for measuring the cross section of standard model processes or for setting upper limits in searches for processes beyond the standard model.

A total of five systems are used for measuring luminosity at CMS. The Pixel Luminosity Telescope (PLT) [2] and Fast Beam Conditions Monitor (BCM1F) [3] are dedicated systems for luminosity measurement, while the hadronic forward calorimeter (HF) uses a dedicated readout on an existing system. These three use a separate data acquisition (DAQ) system, called BRILDAQ, which operates independently of the main CMS readout, so that luminosity measurements can be provided regardless of the current operating state of CMS. In addition, two other methods, the drift tube luminosity (DT) and pixel cluster counting (PCC), use the data from existing parts of the CMS detector to perform a luminosity measurement, using the main CMS DAQ system. The PCC measurement uses the data collected with the standard CMS trigger system [4] with triggers requiring colliding bunches but not any specific event activity ("zero-bias").

Each luminometer reads out a rate of the specific quantities observed in the detector (hits, tracks, clusters, etc.). This rate, R, should be proportional to the instantaneous luminosity, $\mathcal{L}_{\text{inst}}$, with the constant of proportionality given by the visible cross section σ_{vis}:

$$R = \mathcal{L}_{\text{inst}}\sigma_{\text{vis}}. \tag{1}$$

In practice, the luminometers usually exhibit some nonlinear dependence on the instantaneous luminosity or on external factors such as the LHC filling scheme; these nonlinearities need to be corrected to obtain an accurate measurement.

The determination of σ_{vis} is carried out through van der Meer (VdM) scans performed with a dedicated LHC machine setup. In these scans, the two beams are separated and then moved across each other, and the resulting measurement of rate as a function of beam separation can be used to derive the beam overlap width. The absolute luminosity value can subsequently be derived as a function of machine parameters [5] and the measured rate can be used to derive σ_{vis}. Then, this measurement can be used to determine the luminosity in regular physics fills, during which the beam overlap width cannot be measured with the necessary precision. This scan method has previously been used by the LHC experiments for the absolute luminosity scale calibration with high accuracy during a variety of LHC running conditions [6–11].

2 Luminometers at CMS

2.1 The PLT detector

The PLT is a dedicated system for measuring luminosity using silicon pixel sensors, installed at the beginning of 2015 for Run 2. There are a total of 48 sensors arranged into 16 "telescopes", eight at either end of CMS outside the pixel endcap, where each telescope contains three sensor planes arranged nearly parallel to the beam pipe. The sensors measure 8 x 8 mm, divided into 80 rows and 52 columns, although only the central region of the sensors is used to reduce the contribution from background. The readout is performed using the PSI46v2 readout chip. The PLT measures the rate of "triple coincidences", where a hit is observed in all three planes,

typically corresponding to a track from a particle originating at the interaction point. The overall mean rate for PLT (and also in BCM1F) is estimated using the zero-counting method.

Over the course of 2017, accumulated radiation damage in the sensors resulted in a higher-than-expected loss of efficiency in the PLT. The effects of this damage were compensated for by increasing the high voltage applied to the sensors; however, there were still several periods where the PLT had lower efficiency than normal. Corrections for these efficiency losses are applied offline.

2.2 The BCM1F detector

The BCM1F measures both luminosity and machine-induced background (MIB). It consists of a total of 24 sensors mounted on the same carriage as the PLT. For 2017, the sensors in the BCM1F were replaced, and consist of a total of 10 silicon sensors, 10 polycrystalline diamond (pCVD) sensors, and 4 single-crystal diamond (sCVD) sensors. The pCVD and sCVD sensors use split-pad metallization, with each sensor having two readout channels, to keep the overall occupancy low given the expected conditions in Run 2. The BCM1F readout features a fast readout with 6.25 ns time resolution; the precise time measurement, in conjunction with the position of BCM1F 1.8 m from the center of CMS, allows hits from collision products to be separated from hits from MIB, because the incoming background is separated in time from the outgoing collision products.

2.3 The HF measurement

The HF luminosity measurement uses a dedicated readout system installed in the HF calorimeter. The HF provided the primary online luminosity measurement for CMS during Run 1 of the LHC and has continued to provide excellent performance through Run 2. The algorithm used for 2017 uses the sum of the transverse energy E_T (HFET), which provides better performance at higher instantaneous luminosity than the previous occupancy-based algorithm (HFOC).

Two corrections are applied to the primary HFET measurement to account for afterglow effects. "Type 1" corrections account for the signal from a hit spilling over into the next 25 ns bunch crossing (BX) after a colliding bunch, while "type 2" effects account for an exponentially decaying afterglow for several bunches following a colliding bunch due to activation of the surrounding detector material. These effects are measured using data from empty bunches, which should thus have zero luminosity, and corrections are derived and applied to the raw luminosity. The afterglow corrections (combining Type 1 and Type 2) for HFET amount to approximately 4% in the bunch immediately following a colliding bunch and 0.5% in the next following bunch, with the corrections for subsequent bunches less than 0.1%.

2.4 The DT measurement

The DT luminosity measurement uses the rate of muon track stubs in the muon barrel track finder. While the DT measurement is available to the BRILDAQ and is thus available online, the DT algorithm used does not provide bunch-by-bunch measurements and is thus applicable only for the total luminosity measurement. In Run 2 the DT measurement has generally been stable and linear, as long as the track finder itself is not changed, so it provides a complementary offline reference measurement.

2.5 The PCC method

The PCC method uses the rate of pixel clusters in the CMS pixel detector to provide a luminosity measurement. It supplied the primary offline luminosity measurement for CMS in

2015–2016, since the large area of the pixel detector and the relatively low occupancy provides a measurement with good statistical precision, and the stability of the measurement over time is typically good. Because the CMS trigger bandwidth available for collecting the data used for this measurement is limited, the statistical precision for a single 23-second luminosity section is not as high as for the online luminometers, but integrated over longer time periods this is not an issue for the PCC luminosity.

In the PCC measurement, the innermost layer of the pixel detector is excluded because it is significantly affected by dynamic inefficiency effects, where the hit efficiency decreases at higher $\mathcal{L}_{\text{inst}}$ due to the readout chip not being able to process all of the hits. The last part of the 2017 run was affected by problems in the power supply chain resulting in a significant number of modules not operating during this period; these modules are excluded from the final measurement.

As for the HF luminosity, Type 1 and Type 2 corrections are measured and applied to the PCC measurement. Since these corrections varied over the course of the 2017 run, they are measured as a function of time and applied in a time-dependent manner. The afterglow corrections for PCC are in the range 2–5% for the Type 1 corrections and 2–3% averaged over all active bunches for the Type 2 corrections.

3 Van der Meer scans

3.1 Calibration with VdM scans

The instantaneous luminosity for a single colliding bunch i, $\mathcal{L}^i_{\text{inst}}$, can be expressed as a function of beam parameters. If there is no crossing angle between the beams and the beams collide with zero relative separation ("head-on"), the instantaneous luminosity is given by the formula:

$$\mathcal{L}^i_{\text{inst}} = N^i_1 N^i_2 f \int \rho_1(x,y)\rho_2(x,y)\mathrm{d}x\mathrm{d}y = N^i_1 N^i_2 f \int \rho_{x1}(x)\rho_{x2}(x)\mathrm{d}x \int \rho_{y1}(y)\rho_{y2}(y)\mathrm{d}y, \quad (2)$$

where N^i_1 and N^i_2 are the number of protons in the two individual beams for the colliding bunch i, $f = 11246\,\text{Hz}$ is the LHC orbit frequency, and ρ_j is the normalized particle density for the bunch in beam j. The rightmost term of Eq. 2 uses the assumption that ρ can be factorized into independent terms in x and y, $\rho_x(x)$ and $\rho_y(y)$, respectively.

The measurement of the beam currents N is well determined, but the individual proton density functions cannot be directly measured. The VdM method determines the value of the two beam overlap integrals in Eq. 2 by varying the beam separation and measuring the resulting rates:

$$\int \rho_{x1}(x)\rho_{x2}(x)\mathrm{d}x = \frac{R_x(0)}{\int R_x(\delta)\mathrm{d}\delta}, \quad (3)$$

where $R_x(\delta)$ is the rate measured when the two beams are separated in x by a distance δ; a similar equation can be written in y. We then define the beam overlap width Σ_x (and similarly Σ_y) as:

$$\Sigma_x = \frac{1}{\sqrt{2\pi}} \frac{\int R_x(\delta)\mathrm{d}\delta}{R_x(0)}, \quad (4)$$

yielding the final expression for luminosity:

$$\mathcal{L}^i_{\text{inst}} = \frac{N^i_1 N^i_2 f}{2\pi\Sigma_x\Sigma_y}. \tag{5}$$

In practice, the integral in Eq. 4 is evaluated by performing two separate scans in the x and y directions, measuring the rate (normalized by the product of the beam currents) at a certain number of separation steps, fitting the resulting points with a functional form, and using the fitted function to determine the overall integral. This procedure is described in more detail in Ref. [12]. Once Σ_x and Σ_y are determined, then Eq. 1 can be used to obtain the overall visible cross section σ_{vis}. Since Eq. 1 should hold for all beam conditions, the σ_{vis} thus obtained can be used to determine the luminosity in regular beam conditions, not just the special VdM conditions. This is because the detector acceptance should not change between the two conditions; this has been verified in a special fill where the crossing angle was changed in steps from 150 to 120 μrad, and no change in measured σ_{vis} within uncertainties was observed.

In past analyses, the fit was performed using two Gaussian terms plus a constant term, with the constant term accounting for the contribution from MIB and detector noise. However, the constant term was not always well determined in the fit, which could cause stability and consistency issues. Instead, in this analysis, the background contribution is estimated independently, using the measurement of rates in BXes which are filled in one beam but not the other to estimate the contribution from MIB and the measurement of rates in empty BXes in the abort gap for the contribution from detector noise. The estimated background is then subtracted from the raw data before the fit is performed using only two Gaussian terms. This procedure is used for PLT, BCM1F, and HFOC, but not for HFET, since the constant term for HFET is negligibly small (less than 0.1%). For PCC the double Gaussian plus constant fit is still used, since the independent background determination is more difficult in this case.

For a sum of two Gaussians with amplitudes A_1 and A_2 and widths σ_1 and σ_2, the beam overlap width Σ can be calculated using Eq. 4 to be simply $(A_1\sigma_1 + A_2\sigma_2)/(A_1 + A_2)$.

A potential uncertainty in σ_{vis} due to the background subtraction is estimated. First, the statistical uncertainty on the background value is estimated by taking the standard error in the mean value taken over the course of the scan, which amounts to approximately 1–2%. This is then propagated to σ_{vis} by varying the background subtraction by that value, which results in a change in σ_{vis} of approximately 0.01%, so we can conclude that the uncertainty from this source is negligible.

Figure 1 shows an example of the VdM fit procedure for the PLT for an individual bunch with bunch crossing ID number (BCID) 1783.

3.2 2017 scan program

The VdM scans were performed during LHC fill 6016 on July 28th, 2017 at $\sqrt{s} = 13$ TeV. The LHC filling scheme was `Multi_52b_32_12_8_4bpi_13inj` with 32 colliding bunch pairs at the CMS interaction point (IP5) widely spread over the orbit to reduce long-range beam-beam effects and detector afterglow. Special LHC beam optics were used for the fill, with $\beta^* \approx 19$ m and a transverse emittance of $\epsilon_N \approx 3.0$ μm yielding a relatively large beam size of approximately $\sigma_b = 100\,\mu$m. No crossing angle was used for collisions at ATLAS and CMS. The resulting peak pileup is approximately $\mu = 0.6$, much lower than a regular physics fill.

The bunch intensities were approximately 8–9 $\times 10^{10}$ protons per filled bunch, resulting in a total beam intensity of approximately 4.5×10^{12} per beam. The total beam intensities were measured with the DC Current Transformers (DCCT) [13], and the bunch currents were mea-

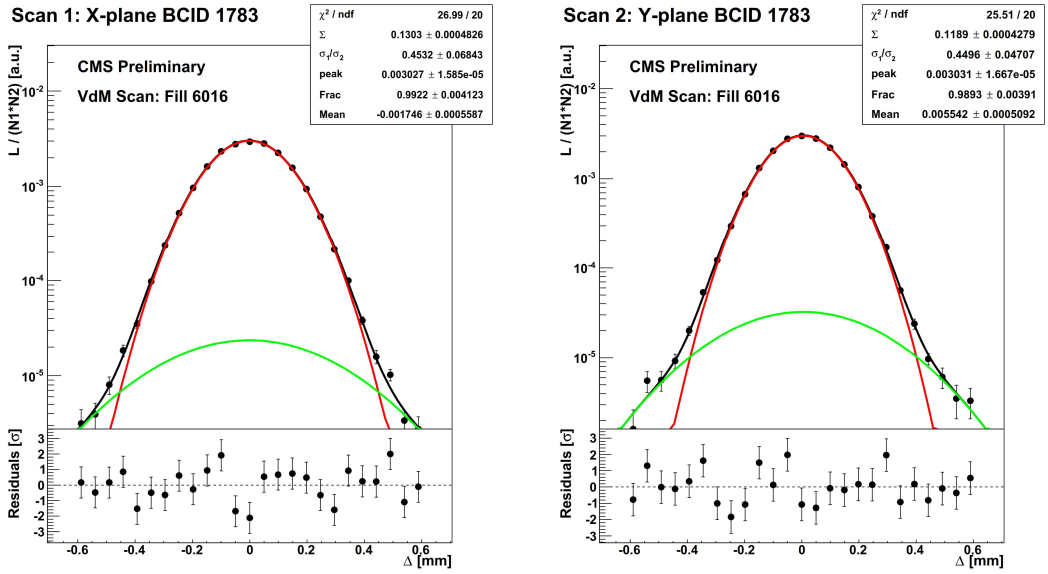

Figure 1: Normalized rates and the resulting fitted double Gaussian scan curves as a function of the beam separation (Δ) for a single bunch as recorded by PLT for a scan in the x (left) and y direction (right). Background subtraction has been applied to the raw data.

sured with the Fast Beam Current Transformers (FBCT) [14] and cross-checked with the Beam Quality Monitors (BQM). The beam orbit was monitored using two systems, the DOROS beam position monitors (BPMs) [15] located near IP5, and the arc BPMs located in the LHC arcs adjacent to CMS. The orbit is also tracked using beam spot movements based on reconstructed vertices. The arc BPM measurements are translated to a beam position at IP5 using the LHC optics file; the specific optics file used for this scan is `R2016c_A19mC19mA19mL24m`.

To ensure a dataset with a high event count for PCC even at large beam separations, CMS gated the zero-bias triggers on 5 bunch pairs (BCIDs 41, 281, 872, 1783, and 2063) and recorded events with a total rate of 20 kHz, using the triggers `HLT_ZeroBias_part[1-8]_v6`.

The CMS VdM scan program consisted of a total of seven x-y scan pairs. Four (#1, #2, #5, and #7) were standard VdM scans, in which the two beams are separated by $6\sigma_b \approx 600\,\mu$m and scanned across one another in a sequence of 25 steps with 30 seconds per step. Scan pair #2 immediately followed #1, in order to measure reproducibility effects, while #5 and #7 occurred later in the fill in order to look for changes over the course of the fill. Scan pairs #3 and #4 were pairs of "beam imaging" scans, in which one beam (beam 1 and beam 2 respectively) is kept fixed at its nominal position while the other is separated and scanned in 19 steps from $+4.5\sigma_b$ to $-4.5\sigma_b$ with 46 seconds per step. Scan pair #6 was an "offset" scan, with the same procedure as the standard scans except that the beams are separated by $\pm 1.5\sigma_b$ in the non-scanning direction, which is not used in this analysis.

In each scan pair, the scan is performed first in the x direction and then in the y direction, with the exception of scan pair #2 which was done the other way around.

A length scale calibration (LSC) was performed immediately prior to scan pair #7 using two

different methods. The first was the "constant separation" scan used in previous years for the CMS length scale calibration, in which the two beams are separated by $1.4\sigma_b$ (approximately equal to 1Σ) and moved together in steps of $1\sigma_b$ across and back, for a total of 10 steps with 70 seconds per step, once in each transverse direction. For 2017, a second "variable separation" scan was added, which follows the scan protocol normally used by ATLAS, in which one beam (starting with beam 1) is moved to $-2.5\sigma_b$ and then a three-point scan is performed with the other beam (starting with beam 2) at a relative position of $-1.25\sigma_b$, 0, and $+1.25\sigma_b$. The position of the first beam is then stepped in five steps to $+2.5\sigma_b$, repeating the three-point scan ("miniscan") at each step. This procedure is repeated four times, with two directions for each of the two beams. Each scan point has a duration of about 46 s.

Figure 2 shows the beam positions for the two beams in the x and y directions as measured by the DOROS BPMs during the scan program, showing the four regular scan pairs, the two beam imaging scan pairs, the offset scan pair, and the two LSC scan programs.

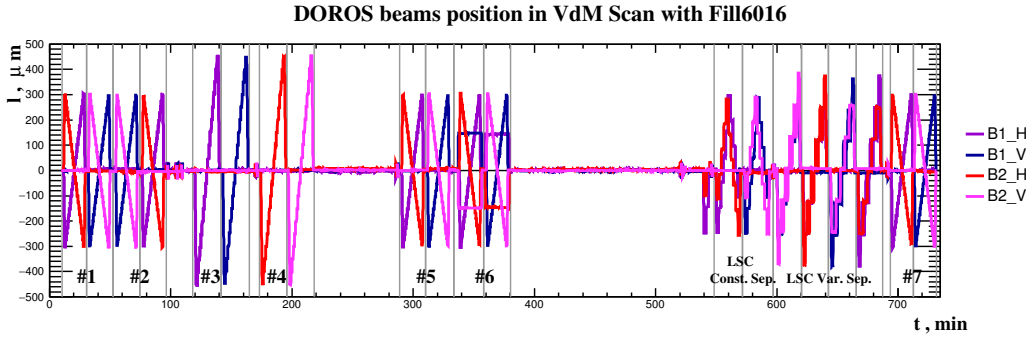

Figure 2: Relative change in beam positions measured by the DOROS BPMs during the 2017 scan program for the two individual beams in the horizontal x and vertical y planes, as a function of the elapsed time from the beginning of the program. The gray vertical lines delimit individual scans.

The beam imaging and offset scans are intended for specific studies on the beam shapes described in Section 4, and they can also be analyzed as traditional van der Meer scans. Both the LSC and beam imaging scans are discussed in detail in Ref. [16].

4 Corrections and systematic uncertainties

There are several systematic effects which affect the beam overlap width measurement, and hence the σ_{vis} extracted from the VdM scan procedure. These effects are measured and, where applicable, corrected as described below, and a systematic uncertainty is assigned on the resulting measured cross section for each source.

4.1 Length scale calibration

The length scale calibration accounts for the fact that when the LHC magnets are used to separate the beams to a desired distance, the actual separation may differ from the nominal separation. In order to measure this effect, a dedicated length scale calibration consisting of two separate scans, as described in Section 3.2, is conducted.

4.1.1 Constant separation scan

In the constant separation scan, the beams are moved together first in the x direction and then in the y direction. The CMS tracker is used to reconstruct the beam spot position and the

resulting position is plotted against the nominal separation; a linear fit is then applied to extract the resulting correction and its uncertainty.

Figure 3 shows the results of the scans in the x and y directions with the forward and backward parts of the scan shown separately. In order to obtain the final length scale correction, the resulting slopes are averaged over the two parts, yielding a slope of 0.994 ± 0.001 in the x and 0.997 ± 0.001 in the y direction. Thus, the measured beam width is reduced by 0.6% and 0.3% in the x and y direction, respectively, resulting in a total reduction in σ_{vis} of $0.9 \pm 0.2\%$, where the uncertainty derives from the statistical uncertainty on the fitted slope.

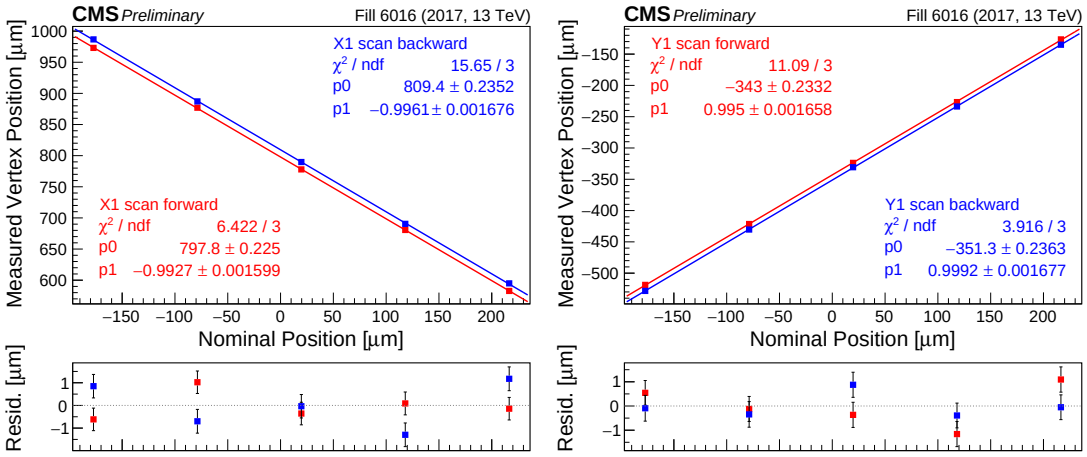

Figure 3: Reconstructed beam spot position as a function of the nominal beam separation in the constant separation LSC scans. Left: scan in the x plane, for the forward (red) and backward (blue) scan directions. Right: same for the y plane. The plots are fitted with a straight line to derive the correction.

The systematic uncertainty in this correction is derived from two sources: the variation in the forward and backward parts of the scan and the effect of orbit drift during the LSC scan (discussed further in Sec. 4.2). Added in quadrature, the total uncertainty is 0.5%. A contribution from the effect of tracker misalignment is considered by comparing prompt reconstructed data and re-reconstructed data in later 2017 running, but as the data are consistent within uncertainties, no additional uncertainty is assigned.

4.1.2 Variable separation scan

In 2017, a new variable separation scan for the LSC was also tried. Like the constant separation scan, this uses the CMS tracker to reconstruct the displacement of the luminous region. However, the variable separation scan is designed to measure the calibration constant for each of the two beams in each of the two directions independently. The calibration data for both horizontal and vertical bumps of beam 1 and beam 2 are presented in Fig. 4. The scale factor which relates the nominal beam displacement to the measured displacement of the luminous centroid is given by the slope of the fitted straight line; the intercept is irrelevant. Because normal VdM scans are performed by displacing the two beams symmetrically in opposite directions, the relevant scale factor in the determination of the beam overlap is the average of the scale factors for beam 1 and beam 2 in each plane, i.e., $(0.9937 + 0.9947)/2 \approx 0.994$ and $(0.9978 + 0.9965)/2 \approx 0.997$ in x and y, respectively. An excellent agreement with the scale factors obtained based on the constant separation scan is observed.

The length scale calibration constants can be then combined from the two independent methods. The impact of orbit drifts during the variable separation scan is evaluated by applying a

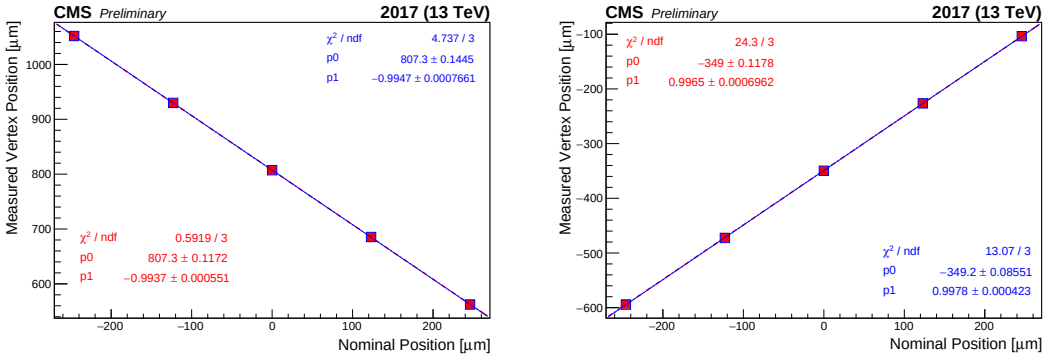

Figure 4: Length scale calibration scan, using the variable separation procedure, for the x (left) and y (right) direction of beam 1 (red) and beam 2 (blue), respectively. Shown is the measured displacement of the luminous centroid as a function of the expected displacement based on the corrector bump amplitude. The line is a linear fit to the data. Errors are of statistical nature.

constant $\pm$ 3 μm drift for all miniscans and found to be 0.3%. The combined total uncertainty on the length scale correction is evaluated to also be 0.3%. The weights of the separate measurements, to be understood in the sense of Ref. [17], are 0.8 and 0.2 for the variable and constant separation scans, respectively. The combined result is found to be robust with respect to the underlying assumption about the extent of the correlation between the two measurements.

4.2 Orbit drift

The orbit drift correction accounts for potential movement of the LHC orbit during the VdM scan. The beam position is measured using two separate beam position monitor systems, the DOROS BPM system and the arc BPMs, with the former used as the primary measurement and the latter as a cross-check. The beam position measurements are taken before and after each scan, as well as at the scan point where the beams are head-on. For each scan, a linear fit is made from the point before the scan to the head-on point and used to derive the correction for the first half of the scan, and similarly a fit from the head-on point to the point after the scan is used to correct the second half of the scan.

Figure 5 shows the measured positions along with the resulting fits. In general, the orbit drift during the 2017 VdM scans is quite small, less than 5 μm for most of the scans; because of the small magnitude of the resulting drift, no correction is applied but the effect of the drift is taken as a systematic uncertainty in the measured cross section, giving an uncertainty of 0.15%.

4.3 The x-y correlations

The VdM scan method assumes that the bunch proton density function is factorizable into independent x- and y-dependent terms. However, this assumption is not strictly valid, and can lead to a biased estimate of the beam overlap area. In order to measure this effect, special beam imaging scans, as described in Section 3.2, are conducted. In these scans, the measured vertex position distributions are used to derive the bunch proton densities, which can then be used to estimate a correction to the visible cross section. More specifically, as the moving beam is scanned across the stationary beam, the resulting two-dimensional vertex distribution can be used to measure the bunch proton density of the stationary beam. The resulting distribution is then fitted with a function to reconstruct the overall distribution.

The simplest model for the bunch proton density that has a correlated spatial dependence is a Gaussian distribution with x-y correlations parametrized by a correlation parameter ϱ:

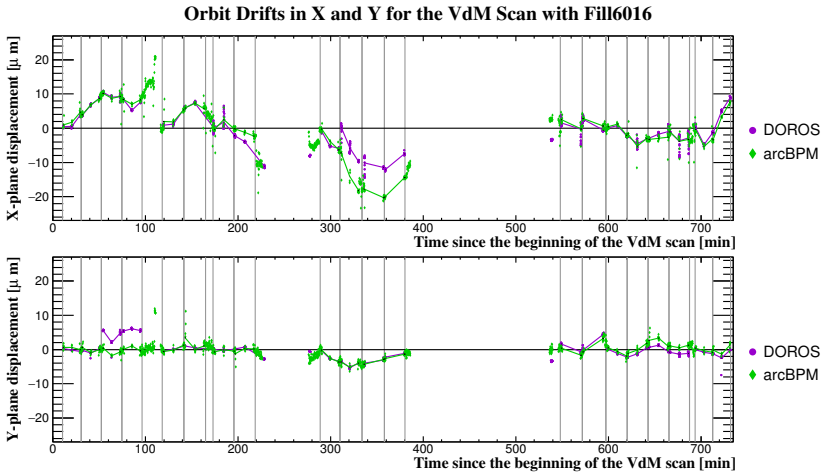

Figure 5: Results of the orbit drift measurement in x (top) and y (bottom). The dots represent the beam position measured at the times when the beams are head-on before, during, and after each scan, as given by the DOROS BPM and arc BPMs in μm. The lines are the fits used to provide the orbit drift correction for each scan step.

$$g(x,y) = \frac{1}{2\pi\sigma_x\sigma_y\sqrt{1-\varrho^2}} \exp\left(\frac{1}{2(1-\varrho^2)}\left[\frac{x^2}{\sigma_x^2} + \frac{y^2}{\sigma_y^2} - \frac{2xy\varrho}{\sigma_x\sigma_y}\right]\right). \tag{6}$$

For this analysis, various functions were evaluated to determine which provided the best fit for the vertex distributions. In the end, the fit is performed using a model that describes the proton density function $\rho(x,y)$ with a main Gaussian component g_M (following the form of Eq. 6) with a large weight w_M, a wide component g_W with a small weight to model wide tails, and a narrow component g_N with a small but negative coefficient $-w_N$ to model a flattened central part:

$$\rho(x,y) = -w_N g_N(x,y) + w_M g_M(x,y) + (1 + w_N - w_M) g_W(x,y). \tag{7}$$

The reconstruction of bunch proton densities from beam imaging scans using a fit model with the weighted sum of two Gaussian distributions is described in detail in Ref. [18].

In order to derive a correction for the measured cross section from the VdM scan, the fitted bunch proton densities are used to simulate VdM scans. The product $\Sigma_x\Sigma_y$ from the Monte Carlo simulation of the VdM scan method can then be compared to the value from a direct integration of the non-factorized bunch proton densities. This yields an estimate of the inaccuracy introduced by using the beam overlap area $\Sigma_x\Sigma_y$, which does not account for the x-y correlations of the bunch proton densities. Multiple simulations are performed to derive the central value of the correction and its statistical uncertainty. Additionally, a Monte Carlo simulation of beam imaging scans is performed to estimate any possible bias from the fit method, and the resulting uncertainty is added to the statistical one.

Figure 6 shows the residuals for the fits to the reconstructed vertex distribution using the fit model from Eq. 7. In general, the fit results are good, although there is some remaining structure, especially in the radial direction.

The overall luminosity correction and uncertainty amount to 0.80% and 0.82%, respectively.

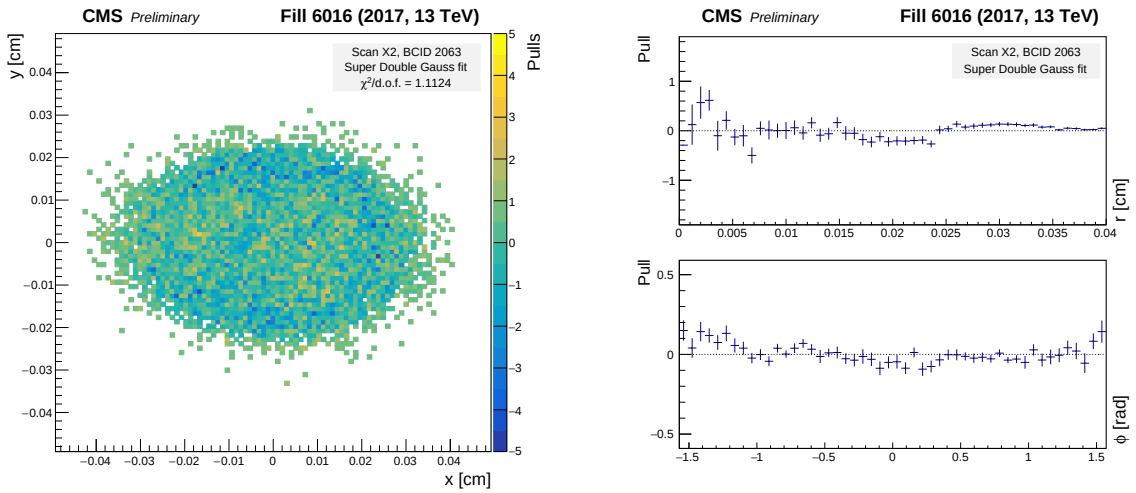

Figure 6: Pull distributions using the model defined in Eq. 7, called previously the "Super Double Gaussian" model. The pull is defined as the difference between the number of measured vertices and the number of vertices predicted by the fit, divided by the statistical uncertainty of the measurement. These plots show the results from the scan constraining beam 1 in x. Left: 2-D pull distribution as a function of x and y position. Right: 1-D projections of the 2-D pull distribution, in slices of constant radius (top) and constant azimuthal angle (bottom).

4.4 Beam-beam effects

Two beam-beam effects are considered in correcting the VdM scan results. The first, beam-beam deflection, accounts for the electrical repulsion of the beams, which increases the lateral separation. It is calculated using the procedure from Ref. [19] and applied as a correction to the beam separation value. The resulting correction is 1.6% with an uncertainty of 0.4%.

The second effect is dynamic-β^*, which accounts for the fact that each beam has a defocusing effect on the other. This effect is measured using beam transport simulations, with a resulting correction of 0.3–0.5% [20]. Because the measured correction shows some variation from scan pair to scan pair, no correction is made, but rather an uncertainty of 0.5% is assigned to cover the maximum variation in σ_{vis} compared with applying only the beam-beam correction. Figure 7 shows the final estimates of the beam-beam deflection and dynamic-β^* corrections.

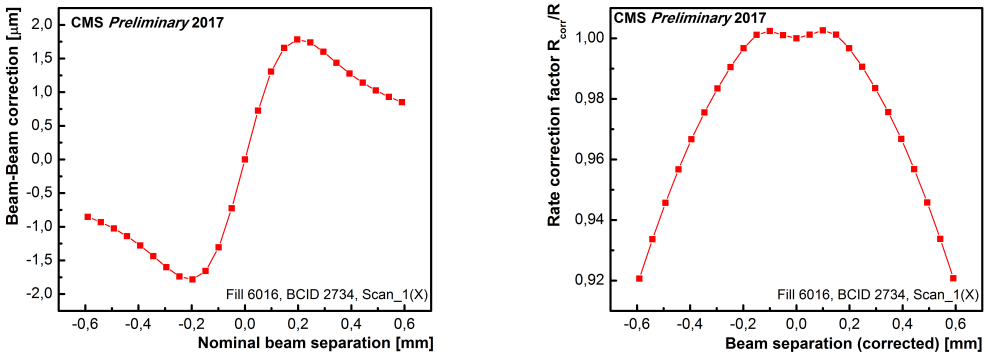

Figure 7: Left: an example of beam-beam deflection estimates as a function of nominal beam separation. Right: an example of the dynamic-β^* effect on rate as a function of the beam separation corrected for the beam-beam deflection.

4.5 Bunch current normalization

Uncertainties in the bunch current used in Eq. 5 arise from two sources. The first arises from the bunch current measurement, which is performed using the FBCTs, which measure the current with a bunch-by-bunch granularity. The DCCT measures the total beam current in each beam; since the absolute scale of this measurement is more precise, the total of the FBCT is normalized to the DCCT measurement. The overall uncertainty in the DCCT measurement is 0.3%, which is taken as the first source of uncertainty. (Uncertainty in the relative bunch-by-bunch measurements is not considered.)

The second uncertainty comes from the presence of "satellite" and "ghost" charges, where the former refers to charge in the colliding bunch crossing but not in the colliding RF bucket, while the latter refers to charge not in any nominally filled bunch slot. These charges will be measured in the FBCT and DCCT measurements, respectively, but do not contribute to the total luminosity, so a correction is needed in order to obtain an accurate value. For the 2017 VdM fill, these contributions are measured using the LHC longitudinal density monitors [21, 22] and determined to be negligibly small; 0.1% is taken as a conservative estimate of the uncertainty from this source. Ghost charge measurement is also achieved using the beam-gas imaging method [23] by comparing the beam-gas rates in beam-empty and empty-empty crossings at the LHCb interaction point (IP8), with consistent results.

5 Visible cross section results

Table 1 shows the measured visible cross sections for the different luminometers. The results are shown with all corrections applied. For DT, the visible cross section is not measured independently, because of the lack of bunch-by-bunch data; rather, DT is cross-calibrated to the PCC result.

Note that σ_{vis} is a property of the individual luminometer geometry, acceptance, and efficiency, and thus depends on the different luminometers. It also depends on the measurement algorithm used, hence the difference in the measured σ_{vis} between HFET and HFOC, as well as the large value for PCC, for which many pixel clusters can be detected for a single collision event.

The measured convolved beam width $\Sigma_{x,y}$, on the other hand, is a function of the beam and thus should be measured to be the same among all the luminometers.

Some variation in the visible cross sections from scan to scan and bunch to bunch is observed. For the scan to scan variation, to cover the possibility of systematic differences between the scan, half the difference between the largest and smallest σ_{vis} among the six scans considered is taken; this percentage value is then averaged over the five luminometers used, resulting in a total of 0.9%. For the bunch to bunch variation, the standard error of the mean after averaging over all bunches is used, resulting in an uncertainty of 0.1%.

After the final calculation of the individual cross sections, we calculate the total integrated luminosity for the periods in the VdM scan fill when no scans were taking place. Since these periods feature a nearly constant luminosity at very low pileup, any effects due to nonlinearity should be negligible and hence the measurements should be equal among the different luminometers. However, in fact, a small difference (approximately 1%) is observed. Figure 8 shows the luminosity for the different luminometers during the VdM fill, in which the remaining residual differences can be observed. In order to correct for this, we rescale the visible cross sections of the five independent luminometers such that they all give an equal luminosity for this fill. Table 2 summarizes the rescaling applied.

Table 1: Summary of measured visible cross sections for the individual luminometers, where the results have been averaged over all bunches and scans. The uncertainty shown includes the effect of the variation among scans; the statistical uncertainty in σ_{vis} for a single scan (after all bunches have been averaged over) is typically approximately 0.1%.

Luminometer	Measured σ_{vis}
BCM1F	$225.6 \pm 1.3\,\mu$b
HFET	$2644.9 \pm 24.1\,\mu$b
HFOC	$838.5 \pm 5.7\,\mu$b
PLT	$297.7 \pm 1.8\,\mu$b
PCC	4.719 ± 0.035 b

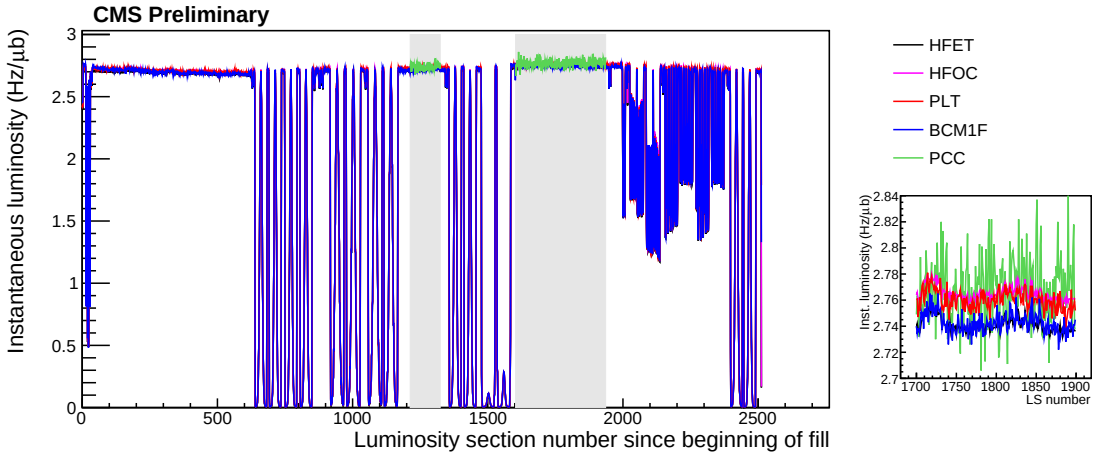

Figure 8: Instantaneous luminosity for the five independent luminometers during the VdM scan fill. The inset shows a zoom in on one of the periods with stable luminosity, in which the slightly different absolute scales of the different luminometers can be observed. The two gray shaded rectangles indicate the periods used to calculate the total integrated luminosity to determine the rescaling.

Note that BCM1F, HF, and PCC only include colliding bunches in the total luminosity, while PLT normally (and also in Fig. 8) includes the sum over all bunches. In physics fills this is a negligible contribution, but given the much lower luminosity in the VdM fill this is not negligible. Hence, in Table 2, we also only use the colliding bunches for PLT for consistency.

We assign a systematic uncertainty of 0.6%, the largest correction applied in the rescaling, as a measure of the uncertainty in the cross-detector calibration in the VdM fill.

6 Detector-specific effects

Over the course of the 2017 run, the individual luminosity detectors were affected by several operational issues. In BCM1F and PLT, radiation damage to the sensors caused a loss of efficiency over the course of the year, while HFET was similarly affected due to gain loss in the PMTs and fibers in HF. PCC was also affected by the previously mentioned power chain issues resulting in a loss of modules in the PCC measurement.

In 2017, CMS was able to take advantage of fast luminosity scans with a small beam separation ("emittance scans") conducted by the LHC to measure these effects. The emittance scans are conducted in the same manner as a VdM scan, but in normal physics conditions over a much shorter time. An emittance scan in 2017 consisted of either 7 or 9 points, with 10 seconds

Table 2: Summary of measured integrated luminosity during stable periods in the VdM fill. The third column indicates the difference between the luminosity and the average; a correction equal to the inverse of this difference is then applied to rescale the σ_{vis} of the luminometer to the average.

Luminometer	Integrated luminosity (nb^{-1})	Difference from average
HFET	28.42	-0.6%
BCM1F	28.45	-0.4%
PLT	28.56	—
HFOC	28.67	+0.3%
PCC	28.71	+0.5%

integration time at each scan point, and a maximum beam separation of approximately $3\sigma_b$, so the entire scan can be conducted in a few minutes. These scans are typically performed at the beginning of the fill and at the end (unless the fill is dumped prematurely). Because of the lesser beam separation and the reduced amount of data at each scan point, the emittance scans do not provide as high a level of precision as the dedicated VdM scans, but they are useful for relative measurements nonetheless. In the VdM scan fill, the results of the emittance scan taken at the beginning of the fill agree within 2% with those of the dedicated VdM scans, although in normal physics conditions, the emittance scans may be less precise because of greater nonlinear effects at higher luminosities.

Figure 9 shows an example of how the emittance scan data were used to measure the gain loss affecting the HFET method. The red line shows the HF aging model derived from studies of the HF PMTs and fibers, while the blue points show the measured HFET visible cross section (averaged over all emittance scans taken in each $5\,\text{fb}^{-1}$ of data), normalized to place it on the same overall scale as the aging model. The two show excellent agreement, giving us confidence that the aging model data can be used to measure and correct for this effect.

Because the emittance scans at the beginning and end of fills are conducted at significantly different single bunch instantaneous luminosity (SBIL), and because individual bunches within a single fill can also exhibit substantially different SBIL, they can also be used to measure the linearity response of a detector. If a detector shows a slope in the measured cross section as a function of SBIL, nonlinear effects are indicated that can also be measured and corrected using the emittance scan data. The detector-specific nonlinearity corrections, derived from the emittance scan data, amount to approximately 0.20–0.45%/(Hz/μb) in PLT, 0.20–0.25%/(Hz/μb) in HFET, and 0.75–0.90%/(Hz/μb) in BCM1F. The corrections vary depending on the bunch train structure used by the LHC, as the nonlinearity observed is different for leading bunches in a train compared to bunches within a train, and also varies depending on time for PLT and BCM1F because they are affected by the changes in efficiency in those detectors during the 2017 running. For PCC and DT no nonlinearity correction is applied.

Although the measurements from the individual luminometers generally agree well, for the purpose of providing a final luminosity measurement, one luminometer is selected, with other luminometers used to fill gaps when the primary luminometer is unavailable due to operational issues. For 2017, the luminosity measurement for a particular time is given by the available luminometer highest in the list HFET, PCC, PLT, BCM1F, and DT. Once the final module quality requirements are applied to PCC, the performance of HFET and PCC was similar in 2017. However, HFET was chosen as the primary method before the final PCC selection became available.

To assess the systematic uncertainty in the HFET corrections, we look at the residual luminosity

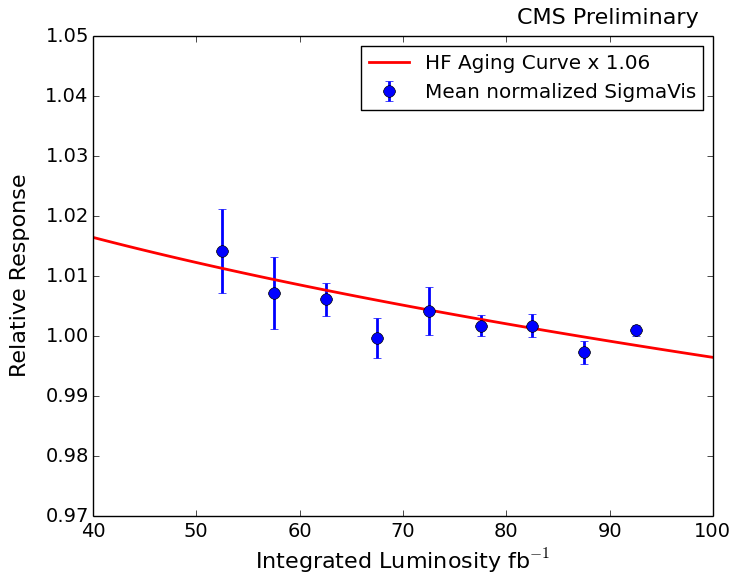

Figure 9: The red curve shows the aging model for the HF, derived from studies on the HF PMTs and fibers and parameterized with a function. The blue points show the average, uncorrected visible cross section derived from emittance scans as a function of integrated luminosity; the smaller uncertainties observed towards the end of the year are because of smaller variation in the σ_{vis} from the individual emittance scan results. Both are scaled arbitrarily to the same scale. Errors shown are statistical.

in the empty bunches after the corrections are applied; the resulting deviation from zero can be used to estimate the uncertainty. For the Type 2 corrections, a 0.3% systematic uncertainty is assigned based on the variation of the residuals over the course of the year. For the type 1 corrections, the systematic uncertainty calculation is affected by the fact that the residuals show a dependence on SBIL. As taking this uncertainty as-is would result in double-counting of linearity effects in HFET, the residuals are instead first corrected using a nonlinearity correction. Once this correction is applied, the remaining variation of 0.2% is assigned as the systematic uncertainty for the Type 1 corrections. Figure 10 shows the residuals from the two correction types (with the nonlinearity correction applied for Type 1).

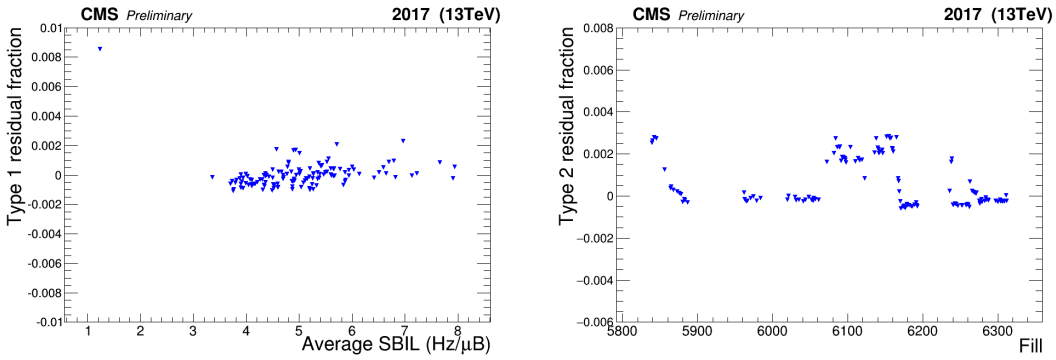

Figure 10: Left: HFET correction Type 1 residual fractions (remaining luminosity in empty bunches after corrections) as a function of average SBIL, after the nonlinearity effect is corrected. Right: Type 2 residual fractions as a function of fill.

The uncertainties in the PCC corrections are evaluated in a similar fashion and the uncertainty is found to be smaller (0.3% for the sum of Type 1 and Type 2), so the HFET uncertainty should

be sufficient to cover the periods when other methods, instead of HFET, were used in the luminosity determination.

7 Cross-detector comparisons

After corrections for known stability and nonlinearity effects are applied to each detector individually, the luminometer measurements can be compared to each other in order to assess the performance of these corrections.

First, the overall consistency of the individual luminometers with respect to each other is evaluated. This is done by taking the ratio of the measured luminosity values for each luminometer pair. Figure 11 shows the results for a particular pair (in this example, BCM1F/HFET). The decrease in BCM1F efficiency caused by radiation damage to the sensors towards the end of 2017 is clearly visible.

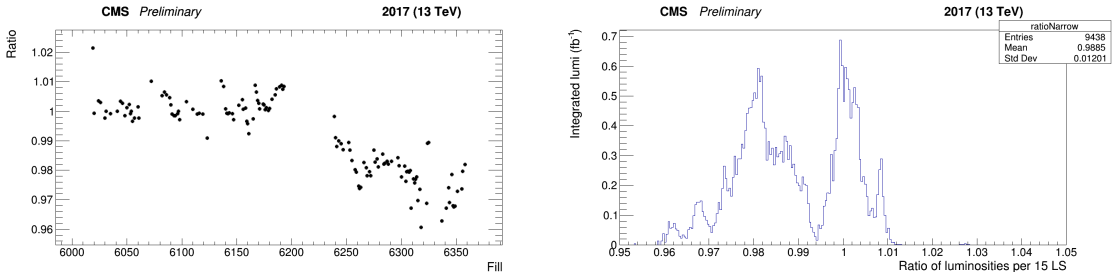

Figure 11: Example of stability comparison for BCM1F/HFET. Left: ratio of the measured luminosity values as a function of fill over the course of 2017. Right: luminosity-weighted binned histogram of the BCM1F/HFET luminosity ratio.

In addition, the linearity response of the different luminometers is also compared in order to assign a systematic uncertainty in the linearity. This is done in two steps. First, for a given fill, the ratio of the luminosity values given by the two luminometers is plotted as a function of average SBIL. This ratio is then fitted with a line and the slope of the fitted line is taken as the relative nonlinearity for those two luminometers for that fill. Then, the extracted slope is plotted as a function of fill, as for the stability. The results for the 2017 data for PLT/HFET are shown in Fig. 12.

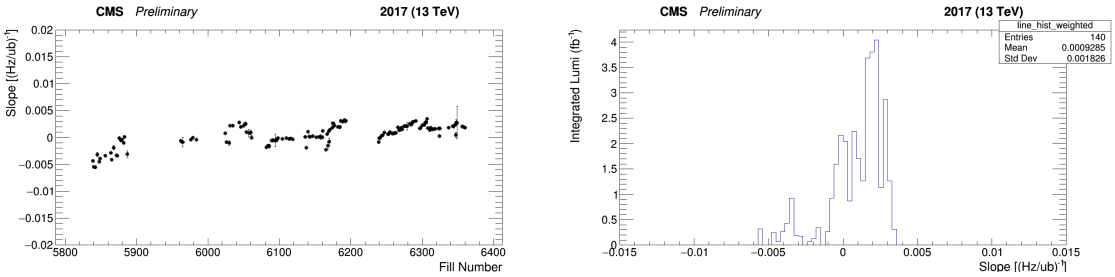

Figure 12: Example of linearity comparison for PLT/HFET. Left: slopes of linear fits to the luminosity ratios as a function of average SBIL versus fill number. Right: luminosity-weighted binned histogram of the slopes.

The overall systematic uncertainty due to stability effects is evaluated to be 0.5%, which is taken from the standard deviation of the HFET/PCC ratio histogram (since HFET and PCC are used for 99.4% of the 2017 luminosity). Figure 13 shows this comparison. For linearity, the systematic uncertainty in the relative slope is taken to be 0.3%/(Hz/μb), which is the largest

standard deviation of the slope histograms among the pairs considered (specifically, for the PLT/PCC comparison, shown in Fig. 14). This uncertainty is then propagated to the overall luminosity profile in 2017, yielding a total systematic uncertainty of 1.5%. Table 3 summarizes the results of the cross-detector comparisons.

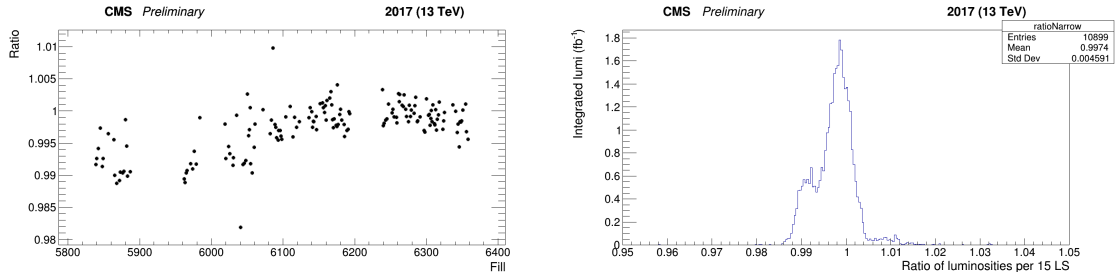

Figure 13: Stability comparison for HFET/PCC, as in Fig. 11. Left: ratio of the measured luminosity values as a function of fill over the course of 2017. Right: luminosity-weighted binned histogram of the HFET/PCC luminosity ratio. The overall stability systematic uncertainty is derived from this comparison.

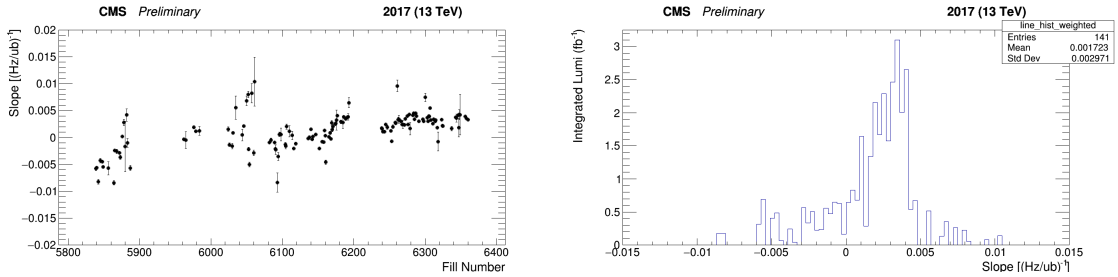

Figure 14: Linearity comparison for PLT/PCC, as in Fig. 12. Left: slopes of linear fits to the luminosity ratios as a function of average SBIL versus fill number. Right: luminosity-weighted binned histogram of the slopes. The overall linearity systematic uncertainty is derived from this comparison.

8 Summary

The analysis of the van der Meer (VdM) scans performed by the CMS Collaboration in July 2017 for the calibration of CMS luminometers to the absolute luminosity scale for proton-proton (pp) collisions at $\sqrt{s} = 13$ TeV has been presented.

Table 4 summarizes the final corrections and systematic uncertainties considered in this analysis. The systematic uncertainties are divided into "normalization" uncertainties; that is, the uncertainties arising from the luminosity calibration in the VdM scan procedure, and "integration" uncertainties, which are the uncertainties arising from the detector operations over the course of the 2017 run.

The dominant uncertainties contributing to the luminosity scale calibration, as described in Section 4, are from the length scale calibration and the x-y correlations of the colliding proton bunch densities. All normalization uncertainties are treated as uncorrelated, giving a total of 1.5% in the luminosity scale calibration.

The integration uncertainty includes the detector-specific uncertainties discussed in Section 6 and the cross-detector stability and linearity uncertainties covered in Section 7. In addition, an uncertainty of 0.5% in the deadtime estimate of the CMS DAQ system is included affecting the recorded integrated luminosity.

Table 3: Summary of cross-detector comparisons. For each pair of detectors compared, each of the following is considered: the mean of the ratio between the two luminosity measurements, the standard deviation of the per-fill luminosity ratios, the mean of the slopes between the two measurements, and the standard deviation of the per-fill slopes.

Luminometer pair	Mean ratio	SD ratio (%)	Mean slope (%/(Hz/μb))	SD slope (%/(Hz/μb))
HFET/PCC	0.9974	0.5	0.07	0.18
PLT/HFET	1.001	0.8	0.09	0.18
PLT/PCC	0.9987	1.0	0.17	0.30
BCM1F/HFET	0.9890	1.2	-0.16	0.16
BCM1F/PCC	0.9869	1.2	-0.09	0.22
DT/HFET	1.002	0.4	0.21	0.14
DT/PCC	0.9979	0.7	0.21	0.26

The integration and normalization uncertainties are treated as uncorrelated. In summary, the total uncertainty in the luminosity measurement in 2017 is 2.3% for CMS data recorded in pp collisions at $\sqrt{s} = 13$ TeV.

Table 4: Summary of the systematic uncertainties entering the CMS luminosity measurement for $\sqrt{s} = 13$ TeV pp collisions. When applicable, the percentage correction is shown.

	Systematic	Correction (%)	Uncertainty (%)
Normalization	Length scale	-0.9	0.3
	Orbit drift	—	0.2
	x-y correlations	+0.8	0.8
	Beam-beam deflection	+1.6	0.4
	Dynamic-β^*	—	0.5
	Beam current calibration	—	0.3
	Ghosts and satellites	—	0.1
	Scan to scan variation	—	0.9
	Bunch to bunch variation	—	0.1
	Cross-detector consistency	0.4–0.6	0.6
Integration	Afterglow (HF)	—	0.2$\oplus$0.3
	Cross-detector stability	—	0.5
	Linearity	—	1.5
	CMS deadtime	—	0.5
	Total		2.3

A Luminosity for the low pileup run

At the end of 2017, CMS also conducted a special run ("Run2017H") in which the beams were adjusted for low pileup running (a pileup of approximately 3). During this run the PCC data is not available; however, the HFET and PLT calibrations are still valid in this regime and so the uncertainties calculated above still apply. Because the overall luminosity was lower in this period, the uncertainty due to linearity effects is correspondingly smaller. The stability has been checked for this period and found to be consistent with the stability in the normal 2017 run. In checking the linearity between HFET and PLT, the offset in the slope distribution is observed to be 0.5%/(Hz/μb), which is higher than the regular 2017 run; this is most likely an artifact of the fact that the luminosity was nearly constant for most of a fill and so the slope is not well determined. Nevertheless, to be conservative, we multiply this slope by the average

SBIL during these fills (0.4) to get an uncertainty of 0.2% for linearity effects. Using this in combination with the other uncertainties yields a total uncertainty of 1.7% for the low-pileup period.

Note that the Run2017H data also includes some periods when the leveling was not in effect and the luminosity was nominal; the 1.7% uncertainty only applies to the low-luminosity running times. The standard 2017 uncertainty should be used for the times with nominal luminosity conditions. The total luminosity delivered by the LHC (under stable beams conditions, with no requirement on the condition of CMS) during times where the low pileup conditions are in effect is 222.4 pb^{-1}.

References

[1] CMS Collaboration, "The CMS experiment at the CERN LHC", *JINST* **3** (2008) S08004, doi:10.1088/1748-0221/3/08/S08004.

[2] P. Lujan, "Performance of the Pixel Luminosity Telescope for luminosity measurement at CMS during Run 2", *PoS* **314** (2017) 504, doi:10.22323/1.314.0504.

[3] M. Hempel, "Development of a Novel Diamond Based Detector for Machine Induced Background and Luminosity Measurements". PhD thesis, DESY, Hamburg, 2017. doi:10.3204/PUBDB-2017-06875.

[4] CMS Collaboration, "The CMS trigger system", *JINST* **12** (2017) P01020, doi:10.1088/1748-0221/12/01/P01020, arXiv:1609.02366.

[5] S. van der Meer, "Calibration of the effective beam height in the ISR", Technical Report CERN-ISR-PO-68-31, 1968.

[6] CMS Collaboration, "CMS luminosity based on pixel cluster counting - Summer 2013 update", CMS Physics Analysis Summary CMS-PAS-LUM-13-001, 2013.

[7] CMS Collaboration, "CMS luminosity calibration for the pp reference run at $\sqrt{s} = 5.02$ TeV", CMS Physics Analysis Summary CMS-PAS-LUM-16-001, 2016.

[8] CMS Collaboration, "CMS luminosity measurement for the 2016 data taking period", CMS Physics Analysis Summary CMS-PAS-LUM-17-001, 2017.

[9] ATLAS Collaboration, "Luminosity determination in pp collisions at $\sqrt{s}$ = 8 TeV using the ATLAS detector at the LHC", *Eur. Phys. J. C* **76** (2016) 653, doi:10.1140/epjc/s10052-016-4466-1, arXiv:1608.03953.

[10] ALICE Collaboration, "Measurement of visible cross sections in proton-lead collisions at $\sqrt{s_{\text{NN}}}$ = 5.02 TeV in van der Meer scans with the ALICE detector", *JINST* **9** (2014) P11003, doi:10.1088/1748-0221/9/11/P11003, arXiv:1405.1849.

[11] LHCb Collaboration, "Precision luminosity measurements at LHCb", *JINST* **9** (2014) P12005, doi:10.1088/1748-0221/9/12/P12005, arXiv:1410.0149.

[12] CMS Collaboration, "CMS luminosity measurement for the 2015 data taking period", CMS Physics Analysis Summary CMS-PAS-LUM-15-001, 2016.

[13] C. Barschel et al., "Results of the LHC DCCT calibration studies", Technical Report CERN-ATS-Note-2012-026 PERF, 2012.

[14] D. Belohrad et al., "The LHC fast BCT system: A comparison of design parameters with initial performance", Technical Report CERN-BE-2010-010, 2010.

[15] M. Gasior, J. Olexa, and R. Steinhagen, "BPM electronics based on compensated diode detectors — results from development systems", *Conf. Proc.* **C1204151** (2012) 44.

[16] M. Zanetti, "Beams scan based absolute normalization of the CMS luminosity measurement", Technical Report CERN-Proceedings-2011-001, 2011.

[17] A. Valassi and R. Chierici, "Information and treatment of unknown correlations in the combination of measurements using the BLUE method", *Eur. Phys. J. C* **74** (2014) 2717, doi:10.1140/epjc/s10052-014-2717-6, arXiv:1307.4003.

[18] M. Klute, C. Medlock, and J. Salfeld-Nebgen, "Beam imaging and luminosity calibration", *JINST* **12** (2017) P03018, doi:10.1088/1748-0221/12/03/P03018, arXiv:1603.03566.

[19] W. Kozanecki, T. Pieloni, and J. Wenninger, "Observation of beam-beam deflections with LHC orbit data", Technical Report CERN-ACC-NOTE-2013-0006, 2013.

[20] A. Babaev, "Beam-dynamic effects at the CMS BRIL van der Meer scans", *JINST* **13** (2018) C03028, doi:10.1088/1748-0221/13/03/C03028.

[21] A. Jeff et al., "Longitudinal density monitor for the LHC", *Phys. Rev. ST Accel. Beams* **15** (2012) 032803, doi:10.1103/PhysRevSTAB.15.032803.

[22] A. Jeff, "A Longitudinal Density Monitor for the LHC". PhD thesis, Liverpool University, 2012.

[23] C. Barschel, "Precision luminosity measurement at LHCb with beam-gas imaging". PhD thesis, RWTH Aachen University, 2014.